Pergamon

Int. J. Heat Mass Transfer. Vol. 38, No. 7, pp. 1305–1315, 1995

0017–9310/95 $9.50+0.00

0017–9310(94)00231–2

Quasi-steady-state three-dimensional temperature distribution induced by a moving circular Gaussian heat source in a finite depth solid

ORONZIO MANCA, BIAGIO MORRONE and VINCENZO NASO†
DETEC—Università degli studi Federico II, Piazzale Tecchio, 80125 Napoli, Italy

(*Received* 23 *July* 1993 *and in final form* 16 *July* 1994)

Abstract—An analytical solution to the three-dimensional quasi-stationary problem in a finite depth and width solid with a circular Gaussian moving heat source at the body surface is developed and analyzed. The temperature distribution and the axial coordinate at which the maximum midplane temperature is achieved are presented as a function of Peclet number, solid thickness and width. The dependence of the maximum midplane temperature on the process parameters is highlighted. Combinations of process parameters for which the solution to the three-dimensional problem can be approximated by those to simpler models are pointed out.

INTRODUCTION

Heat transfer analysis is of crucial importance in materials manufacturing and processing [1, 2]. This is also due to the availability of new materials and to the use of innovative processes employing laser and electron beam. These high power beams are now widely used in many applications, such as welding, drilling, cutting, heat treating of metals and manufacturing of electronic components. It is, therefore, necessary to study the conductive thermal fields induced in the solid by a moving heat source.

Most theoretical studies made reference to the infinite or semi-infinite body. One of the first analytical solutions was derived by Jaeger [3] for the temperature distribution in a semi-infinite solid with a surface rectangular moving heat source. Rosenthal [4] developed the theory for the moving heat sources and presented the exact solutions for differently shaped moving spots on both semi-infinite and finite bodies. The same solutions for a semi-infinite solid were obtained by Carslaw and Jaeger [5] by using the heat source method.

As far as a Gaussian distribution of the laser and electron beam heat flux is assumed, solutions to the temperature field induced in semi-infinite solids by a Gaussian circular moving heat source have been derived by several authors. Cline and Anthony [6] correlated the cooling rate and the melting depth to the size, the velocity and the power of the spot. Chen and Lee [7] took into account the effects on the temperature profiles of the scanning velocity, the beam radius and the beam shape. Sanders [8] presented a general solution and found the conditions under which the solution, as a function of its normalized velocity, can be used; the author extended the analysis to a Gaussian pulsed moving heat source. The same problem was analyzed by Modest and Abakians [9]. Nissim *et al.* [10] presented an analytical solution for a moving elliptical Gaussian heat source, which accounted for the temperature dependence of thermal conductivity. Their model was generalized by a numerical algorithm set up by Moody and Hendel [11].

When the order of magnitude of the penetration depth is the same as that of the body thickness, the solid can no longer be assumed as a semi-infinite one. Pittaway [12] solved the temperature distribution in an adiabatic thin plate with either stationary or moving circular Gaussian heat source. For the same heat sources Lolov [13] derived the solution to the three-dimensional linear problem in a finite depth and indefinite width adiabatic body, whereas Tsai and Hou [14] analyzed, for a solid whose dimension along the direction perpendicular to that of the motion was finite, the thermal characterization of the welding both at steady-state and transient conditions. The same problem was solved by Kar and Mazumder [15]; their model allowed the determination of the transient three-dimensional temperature distribution in a solid whose thermophysical properties, except the thermal diffusivity, were assumed to be time dependent.

In spite of the papers published on the subject, the authors think that the three-dimensional problem in a solid heated by a moving circular Gaussian heat source and having a finite dimension along the direction orthogonal to that of the motion has not been thoroughly studied.

† Author to whom correspondence should be addressed.

NOMENCLATURE

c_{ms}	coefficient, equation (10)
$G(\cdot\|\cdot)$	Green's function
H	thickness of the solid
k	thermal conductivity
l	width of the solid
m	index of series
Pe	Peclet number, equation (16)
p_{ms}	coefficient in series, equation (8)
q	surface heat flux
r	radius of Gaussian spot
s	index of series
t	time
T	temperature rise
T^*	dimensionless temperature, equation (20)
v	heat source–solid relative velocity
$\mathbf{v}$	heat source–solid vectorial relative velocity
W	function, equation (5)
x, y, z	Cartesian coordinates aboard of the heat source
X, Y, Z	dimensionless Cartesian coordinates, equation (16)
$\bar{X}$	axial coordinate of maximum temperature.

Greek symbols

α	thermal diffusivity
τ	time, in Green's function.

Subscripts

f	at $x \to -\infty$
0	at $x = 0$
max	maximum.

Superscripts

+	dimensionless
′	dummy spatial variable.

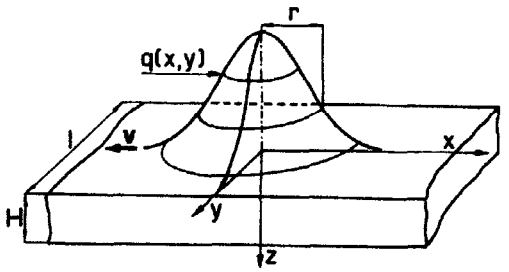

Fig. 1. Geometry and coordinates of the system.

In this paper an analytical solution to the three-dimensional quasi-stationary problem in a finite depth and width solid with a circular Gaussian moving heat source at the body surface is developed and analyzed. It can be used for the prediction of the process parameters in heat treatments. The temperature distribution and the axial coordinate at which the maximum midplane temperature is achieved are presented as a function of Peclet number, solid thickness and width. The dependence of the maximum midplane temperature on the process parameters is highlighted.

MATHEMATICAL DESCRIPTION AND SOLUTION

Consider a circular Gaussian heat source, moving at a constant relative velocity $\mathbf{v}$ over the surface of a solid. The depth and the width of the solid are finite. The geometry and the coordinates are schematically shown in Fig. 1. The body is isotropic and homogeneous; there is no heat generation inside it. In the coordinates system moving with the heat source, according to Rosenthal [4], a mathematical statement of the quasi-steady-state three-dimensional problem is the solution to

$$\frac{\partial^2 T}{\partial x^2} + \frac{v}{\alpha}\frac{\partial T}{\partial x} + \frac{\partial^2 T}{\partial y^2} + \frac{\partial^2 T}{\partial z^2} = 0$$

$$0 \leqslant |x| < +\infty \quad 0 \leqslant |y| \leqslant l/2 \quad 0 \leqslant z \leqslant H \tag{1a}$$

$$T(x \to -\infty, y, z) = T_f \quad 0 \leqslant |y| \leqslant l/2 \quad 0 \leqslant z \leqslant H \tag{1b}$$

$$T(x \to +\infty, y, z) = 0 \quad 0 \leqslant |y| \leqslant l/2 \quad 0 \leqslant z \leqslant H \tag{1c}$$

$$\frac{\partial T(x, \pm l/2, z)}{\partial y} = 0 \quad 0 \leqslant |x| < +\infty \; 0 \leqslant z \leqslant H \tag{1d}$$

$$-k\frac{\partial T(x, y, 0)}{\partial z} = q_0 \exp\left(-\frac{x^2 + y^2}{r^2}\right)$$

$$0 \leqslant |x| < +\infty \quad 0 \leqslant |y| \leqslant l/2 \tag{1e}$$

$$\frac{\partial T(x, y, H)}{\partial z} = 0 \quad 0 \leqslant |x| < +\infty \quad 0 \leqslant |y| \leqslant l/2 \tag{1f}$$

where T is the temperature rise above the temperature at $x \to -\infty$. Thermal properties k and α are assumed to be independent of temperature and position.

The solution to the conductive problem (1) can be derived considering the correspondent transient problem with the initial condition

$$T(x, y, z, 0) = 0 \tag{2}$$

and the following transformation

$$T(x,y,z,t) = W(x,y,z,t)\exp\left(-\frac{v}{2\alpha}x-\frac{v^2}{4\alpha}t\right). \quad (3)$$

The function W can be obtained by using the Green's function [16–18]. Combining the relations given by Beck *et al.* [18] for an infinite domain and for finite domains with adiabatic surfaces, for a three-dimensional region one can write

$$G(x,y,z,t|x',y',z',\tau) = \frac{\exp\left[-\frac{(x-x')^2}{4\alpha(t-\tau)}\right]}{Hl[4\alpha\pi(t-\tau)]^{1/2}/2}$$
$$\times\left\{1+2\sum_{m=1}^{\infty}\exp\left[-\frac{4m^2\pi^2\alpha(t-\tau)}{l^2}\right]\cos\frac{2m\pi y}{l}\cos\frac{2m\pi y'}{l}\right\}$$
$$\times\left\{1+2\sum_{s=1}^{\infty}\exp\left[-\frac{s^2\pi^2\alpha(t-\tau)}{H^2}\right]\cos\frac{s\pi z}{H}\cos\frac{s\pi z'}{H}\right\}. \quad (4)$$

From Beck *et al.* [18, p. 51, equation (3.46)] we obtain

$$W(x,y,z,t) = \frac{q_0\alpha}{Hlk/2}\int_{\tau=0}^{t}\int_{x'=-\infty}^{\infty}\int_{y'=0}^{l/2}$$
$$\times\exp\left(-\frac{x'^2+y'^2}{r^2}+\frac{v}{2\alpha}x'+\frac{v^2}{4\alpha}\tau\right)$$
$$\times\frac{\exp\left[-\frac{(x-x')^2}{4\alpha(t-\tau)}\right]}{[4\alpha\pi(t-\tau)]^{1/2}}\left\{1+2\sum_{m=1}^{\infty}\right.$$
$$\left.\times\exp\left[-\frac{4m^2\pi^2\alpha(t-\tau)}{l^2}\right]\cos\frac{2m\pi y}{l}\cos\frac{2m\pi y'}{l}\right\}$$
$$\times\left\{1+2\sum_{s=1}^{\infty}\exp\left[-\frac{\pi^2s^2\alpha(t-\tau)}{H^2}\right]\right.$$
$$\left.\times\cos\frac{s\pi z}{H}\cos\frac{s\pi z'}{H}\right\}dy'\,dx'\,d\tau \quad (5)$$

and, by substituting equation (5) into equation (3), we get

$$T(x,y,z,t) = \frac{q_0\alpha}{Hlk/2}\exp\left(-\frac{v}{2\alpha}x\right)$$
$$\times\int_{x'=-\infty}^{\infty}\exp\left(-\frac{x'^2}{r^2}+\frac{v}{2\alpha}x'\right)$$
$$\times\int_{y'=0}^{l/2}\exp\left(-\frac{y'^2}{r^2}\right)$$
$$\times\int_{\tau=0}^{t}\frac{\exp\left[-\frac{(x-x')^2}{4\alpha(t-\tau)}\right]}{[4\alpha\pi(t-\tau)]^{1/2}}\exp\left[-\frac{v}{4\alpha}(t-\tau)\right]$$
$$\times\left\{1+2\sum_{m=1}^{\infty}\exp\left[-\frac{4m^2\pi^2\alpha(t-\tau)}{l^2}\right]\cos\frac{2m\pi y}{l}\cos\frac{2m\pi y'}{l}\right\}$$
$$\times\left\{1+2\sum_{s=1}^{\infty}\exp\left[-\frac{s^2\pi^2\alpha(t-\tau)}{H^2}\right]\cos\frac{s\pi z}{H}\right\}d\tau\,dy'\,dx'. \quad (6)$$

The integration over the time can be carried out for the asymptotic quasi-steady-state condition ($t\to\infty$). From Abramowitz and Stegun [19, p. 1026, equation (29.3.84)] one has

$$\int_{\tau=0}^{\infty}\frac{\exp\left[-\frac{(x-x')^2}{4\alpha(t-\tau)}\right]}{[4\alpha\pi(t-\tau)]^{1/2}}\exp\left[-\frac{p_{ms}v^2}{4\alpha}(t-\tau)\right]d\tau$$
$$=\frac{1}{vp_{ms}}\exp\left(-\frac{p_{ms}|x-x'|v}{2\alpha}\right) \quad (7)$$

where

$$p_{ms} = \begin{cases} 1 & \text{for } m=s=0 \\ \left[1+\left(\frac{4m\pi\alpha}{vl}\right)^2\right]^{1/2} & \text{for } m>0 \text{ and } s=0 \\ \left[1+\left(\frac{2s\pi\alpha}{vH}\right)^2\right]^{1/2} & \text{for } m=0 \text{ and for } s>0 \\ \left[1+\left(\frac{2s\pi\alpha}{vH}\right)^2+\left(\frac{4m\pi\alpha}{vl}\right)^2\right]^{1/2} & \text{for } m>0 \text{ and } s>0. \end{cases} \quad (8)$$

Substituting expression (7) into equation (6) gives, for quasi-steady-state condition

$$T(x,y,z) = \frac{8q_0\alpha}{Hlkv}\exp\left(-\frac{v}{2\alpha}x\right)$$
$$\times\sum_{m=0}^{\infty}\sum_{s=0}^{\infty}c_{ms}\cos\frac{2m\pi y}{l}\cos\frac{s\pi z}{H}$$
$$\times\int_{y'=0}^{l/2}\exp\left(-\frac{y'^2}{r^2}\right)\cos\frac{2m\pi y'}{l}dy'$$
$$\times\int_{x'=-\infty}^{\infty}\exp\left(-\frac{x'^2}{r^2}+\frac{v}{2\alpha}x'\right)$$
$$\times\exp\left(-\frac{p_{ms}|x-x'|v}{2\alpha}\right)dx' \quad (9)$$

where

$$c_{ms} = \begin{cases} \frac{1}{4} & \text{for } m = s = 0 \\ \dfrac{1}{2p_{m0}} & \text{for } m > 0 \\ \dfrac{1}{2p_{0s}} & \text{for } s > 0 \\ \dfrac{1}{p_{ms}} & \text{for } m > 0 \text{ and } s > 0 \end{cases} \quad (10)$$

with p_{ms} defined in equation (8).

The integrals over the dummy variable x' can be evaluated in the following way. For $x' < x$ we get

$$I_1 = \exp\left(-\frac{vp_{ms}x}{2\alpha}\right)\int_{x'=-\infty}^{x} \times \exp\left[-\left(\frac{x'^2}{r^2} - \frac{v}{2\alpha}(1+p_{ms})\,x'\right)\right]dx' \quad (11)$$

and for $x' > x$ we obtain

$$I_2 = \exp\left(\frac{vp_{ms}x}{2\alpha}\right)\int_{x'=x}^{\infty} \exp\left[-\left(\frac{x'^2}{r^2} - \frac{v}{2\alpha}(1-p_{ms})\,x'\right)\right]dx'. \quad (12)$$

According to Abramovitz and Stegun [19, p. 302, equation (7.4.2)], one can obtain for integrals (11) and (12):

$$I_1 = \frac{\sqrt{\pi}r}{2}\exp\left[-\frac{vx}{2\alpha}p_{ms}\right]\exp\left[\left(\frac{vr}{4\alpha}\right)^2(1+p_{ms})^2\right] \times \operatorname{erfc}\left[\frac{vr}{4\alpha}(1+p_{ms}) - \frac{x}{r}\right] \quad (13)$$

$$I_2 = \frac{\sqrt{\pi}r}{2}\exp\left[\frac{vx}{2\alpha}p_{ms}\right]\exp\left[\left(\frac{vr}{4\alpha}\right)^2(1-p_{ms})^2\right] \times \operatorname{erfc}\left[\frac{x}{r} - \frac{vr}{4\alpha}(1-p_{ms})\right]. \quad (14)$$

The integrals over the variable y' can be evaluated in closed form only for $m = 0$. In fact for $m = 0$ we get

$$\int_{y'=0}^{l/2}\exp\left(-\frac{y'}{r^2}\right)dy' = \frac{r\sqrt{\pi}}{2}\operatorname{erf}\left(\frac{l}{2r}\right). \quad (15)$$

Introducing the following dimensionless variables:

$$X = \frac{x}{r} \quad Y = \frac{y}{r} \quad Z = \frac{z}{r} \quad H^+ = \frac{H}{r}$$

$$l^+ = \frac{l}{r} \quad Pe = \frac{vr}{2\alpha} \quad T^+ = \frac{T}{(q_0 r/k)} \quad (16)$$

and substituting expressions (13) and (14) in equation (9), with

$$p_{ms} = \left\{1+\left(\frac{\pi}{Pe}\right)^2\left[\left(\frac{2m}{l^+}\right)^2 + \left(\frac{s}{H^+}\right)^2\right]\right\}^{1/2} \quad (17)$$

we finally obtain the quasi-steady-state temperature distribution

$$T^+(X, Y, Z, l^+, H^+, Pe) = \frac{2\sqrt{\pi}}{H^+ l^+ Pe} \times \sum_{m=0}^{\infty}\sum_{s=0}^{\infty} c_{ms}\cos\frac{2m\pi Y}{l^+}\cos\frac{s\pi Z}{H^+} \times \left\{\exp\left[Pe(1+p_{ms})\left(\frac{Pe}{4}(1+p_{ms}) - X\right)\right] \times \operatorname{erfc}\left[\frac{Pe}{2}(1+p_{ms}) - X\right] + \exp\left[Pe(1-p_{ms})\left(\frac{Pe}{4}(1-p_{ms}) - X\right)\right] \times \operatorname{erfc}\left[X - \frac{Pe}{2}(1-p_{ms})\right]\right\} \times \int_{Y'=0}^{l^+/2}\exp(-Y'^2)\cos\frac{2m\pi Y'}{l^+}\,dY' \quad (18)$$

where c_{ms} has been defined in equation (10), with p_{ms} in the dimensionless form (17) and defined as in equation (8). The dimensionless integral over y' for $m = 0$ is

$$\int_{Y'=0}^{l^+/2}\exp(-Y'^2)\,dY' = \frac{\sqrt{\pi}}{2}\operatorname{erf}\left(\frac{l^+}{2}\right). \quad (19)$$

It is worthwhile noting that the asymptotic value attained by the temperature is the final downstream temperature, whose value, $\operatorname{erf}(l^+/2)\pi/(2\ Pe\ H^+ l^+)$, can be evaluated by a global energy balance. Dimensionless temperatures derived from equation (18), when referred to the term $2Pe\ H^+ l^+/\pi$, have, at any width of the body, a unique asymptotic value. In the following, results will be presented in terms of

$$T^* = T^+ 2Pe\, H^+ l^+/\pi. \quad (20)$$

RESULTS

The solution to the problem has been analyzed in the Peclet number, dimensionless thickness and half-width of the solid range 0.1–10, which is of higher interest in the applications. Temperature values were derived with an approximation not less than 10^{-5}. The complementary error function in equation (18) was taken from ref. [20, p. 108] when its argument is less than 3.5 and from ref. [21, p. 388] when the argument is not less than 3.5. The temperature distribution and the coordinate at which maximum temperature is attained were determined iteratively at an approximation not less than 10^{-5} and 10^{-6}, respectively. For the sake of brevity, in the following the superscript '+' is omitted when dimensionless temperature, thickness and width are cited.

The dimensionless temperature profiles as a function of the dimensionless spatial coordinate along the motion, X, at various Peclet numbers and for $H = 0.1$,

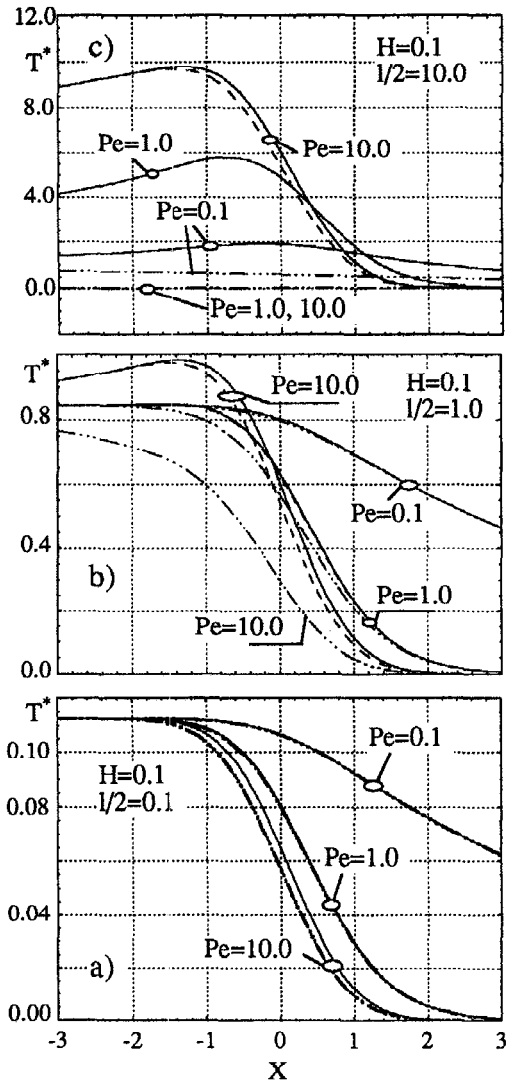

Fig. 2. Temperature profiles (——— $Z = Y = 0.0$;— — — $Z = H, Y = 0.0$;— · · · — $Z = H, Y = l/2$) vs axial coordinate for $H = 0.1$ and $Pe = 0.1$, 1, 10: (a) $l/2 = 0.1$; (b) $l/2 = 1$; (c) $l/2 = 10$.

are reported in Fig. 2. Figure 2(a) shows that, in a solid whose half-width is one-tenth of the radius of Gaussian spot ($l/2 = 0.1$), there is no maximum in temperature profiles, both at the upper and at the lower surface. As far as the dependence on the Peclet number is concerned, one can notice that at $Pe = 0.1$ and 1 the temperature distribution in the YZ planes is practically uniform, whereas at $Pe = 10$ temperature is still independent of Y, but it turns out to be fairly dependent on Z. One can, therefore, conclude that in a thermally thin and narrow body, the thermal analysis can be reduced to that of a one-dimensional field dependent on the axial coordinate. We can also notice that the upstream diffusion of the heat decreases with increasing Peclet number. This is due to the fact that the higher the velocity the lower the contribution of the diffusion and the higher that of the convection to the heat removal. Figure 2(b) points out that in a thermally wider solid ($l/2 = 1$) the temperature is still independent of Y and Z, no maximum being attained at the lowest Peclet number. At $Pe = 1$ the temperature is still independent of the depth and it exhibits a maximum at about $X = -1.8$; on the contrary, temperature varies along Y at the bottom surface. At $Pe = 10$ midplane temperatures are slightly dependent on Z and attain their maximum values at about $X = -1.3$ for $Z = 0$ and at $X = -1.4$ for $Z = H$. Furthermore, the figure points out some dependence of the temperature on Y both on the top and bottom surfaces. Figure 2(c) shows that, in the thermally widest solid ($l/2 = 10$), midplane temperature profiles exhibit a maximum at all Peclet numbers. We can also notice that, the greater the Peclet number, the greater the distance from the origin at which the maximum temperature is attained. One can finally observe from Fig. 2 that, at all Peclet numbers, the greater the width of the solid the higher the dependence of the temperature on Y, and one can also conclude that, at any width, the body can be considered thermally thin.

The spatial distribution along X of the dimensionless temperature, at various Peclet numbers and for $H = 1$, is reported in Fig. 3. Figure 3(a) shows that, in a body 10 times thicker than that in Fig. 2, the solid upper surface temperature profiles exhibit a maximum at any Peclet number and that temperature gradients along Y are negligible, whereas they are remarkable along the Z axis. Temperature profiles and their asymptotic values are very similar to those peculiar to a two-dimensional problem, since in this case ($l/2 = 0.1$) the heat flux can be assumed to be independent of Y. At the lowest Peclet number temperature profiles are similar to those in the 10-times-thinner body [Fig. 2(a)]. However, one can notice a slight difference between the temperature of the upper and the lower solid surfaces in the thicker solid. At higher Peclet numbers the temperature becomes more dependent on the depth and its distribution on the upper surface is strongly dependent on the axial coordinate. When the ratio of the solid width to the radius of Gaussian spot is higher [Fig. 3(b) and (c)], the surface heat flux can no longer be assumed to be uniform along Y. Some temperature gradients along the width can be noticed only at $Pe = 10$ for $l/2 = 1$, whereas they are displayed at all Peclet numbers for $l/2 = 10$. In this case temperature profiles are very similar to those exhibited by a thermally finite depth and indefinite width solid, according to that reported by Lolov [13].

The dimensionless temperature profiles as a function of the dimensionless spatial coordinate along the motion, X, at various Peclet numbers and for $H = 10$, are reported in Fig. 4. It shows that, at any dimensionless width of the body, its bottom surface is practically undisturbed for $Pe = 1$ and $Pe = 10$; for $Pe = 0.1$ the thermal penetration depth is higher than the thickness of the body at $l/2 = 0.1$ and $l/2 = 1$ [Fig.

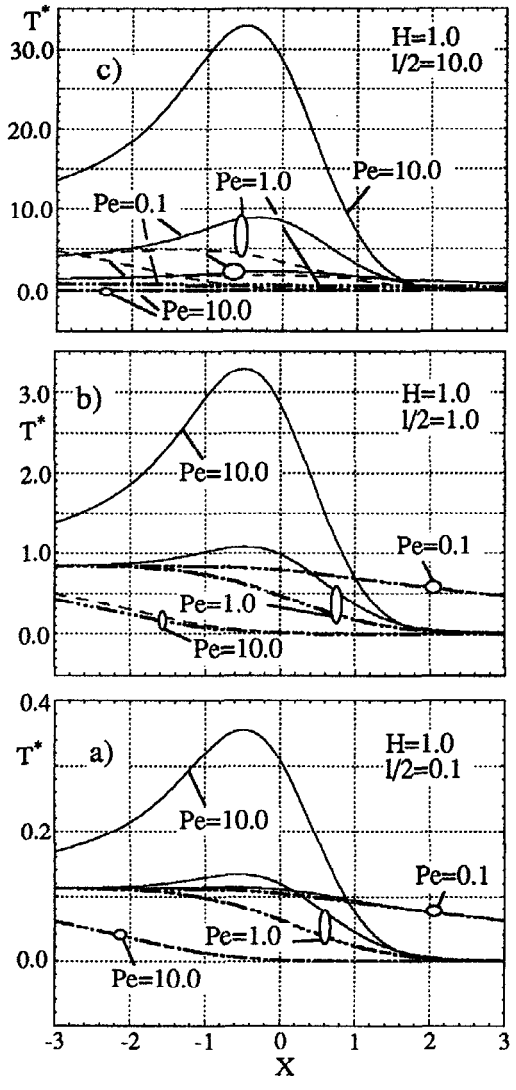

Fig. 3. Temperature profiles (——— $Z = Y = 0.0$; ——— $Z = H, Y = 0.0$; —·—·— $Z = H, Y = l/2$) vs axial coordinate for $H = 1$ and $Pe = 0.1$, 1, 10: (a) $l/2 = 0.1$; (b) $l/2 = 1$; (c) $l/2 = 10$.

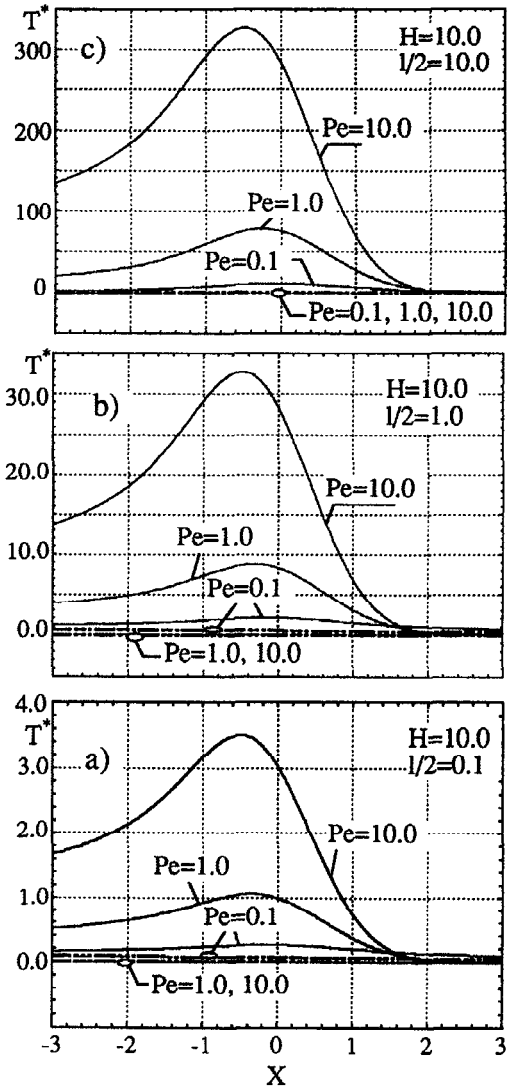

Fig. 4. Temperature profiles (——— $Z = Y = 0.0$; ——— $Z = H, Y = 0.0$; —·—·— $Z = H, Y = l/2$) vs axial coordinate for $H = 10$ and $Pe = 0.1$, 1, 10: (a) $l/2 = 0.1$; (b) $l/2 = 1$; (c) $l/2 = 10$.

4(a) and (b), respectively], whereas at $l/2 = 10$ [Fig. 4(c)] the solid behaves like a semi-infinite one in the X range reported in Fig. 4(c).

The spatial distribution of the dimensionless temperature, for physically meaningful thickness and width of the solid ($H = 1, l/2 = 1$) and different values of the Peclet number, is reported in Fig. 5. At the lowest value of the Peclet number [Fig. 5(a)] one can notice that, beyond a certain value of the axial coordinate, the temperature is nearly independent of Y and Z. This is due to the fact that, when $Pe = 0.1$, the diffusive contribution to the heat removal is by far higher than the convective one in an adiabatic solid, whose dimensions in YZ planes are finite compared to the radius of the Gaussian spot. Notice the wide extension of the downstream region at a uniform temperature, whose asymptotic value is attained at about $X = -1.3$ [see also Fig. 3(b)]. Figure 5(b) and (c) shows that increasing Peclet number determines the increasing dependence of the temperature on all the spatial coordinates. It is worthwhile noting in Fig. 5(c) the marked dependence of the temperature on the Z coordinate, when convective effects are considerably higher than diffusive effects ($Pe = 10$). Furthermore, as is already shown in Fig. 3(b), Fig. 5 points out that, at any depth, the upstream X values at which the solid can be considered thermally undisturbed decrease with increasing Peclet number and the difference between their values on the top and bottom surface of the solid increases with increasing Peclet number.

The dimensionless temperature as a function of the spatial coordinates, for $H = 1$, $l/2 = 10$ and $Pe = 1$, is plotted in Fig. 6. The figure points out that, in

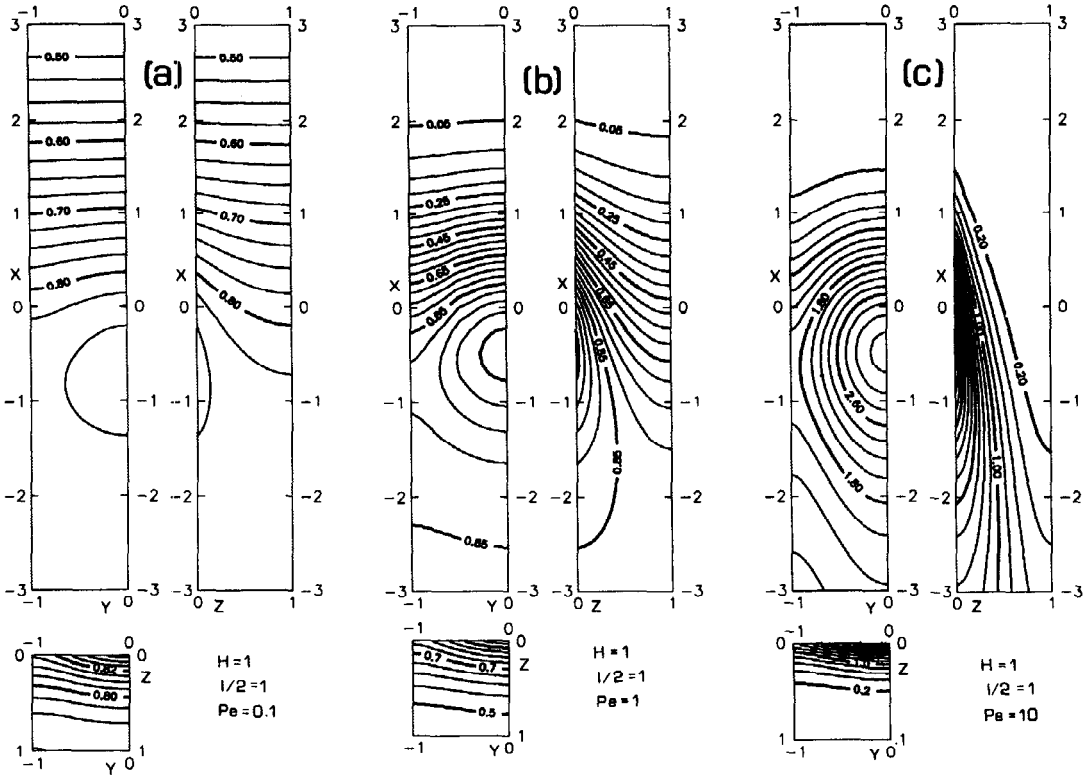

Fig. 5. Spatial distribution of the dimensionless temperature for $H = 1$ and $l/2 = 1$: (a) $Pe = 0.1$; (b) $Pe = 1$; (c) $Pe = 10$.

a thermally wide body, the temperature distribution along Y is very similar to that in a plate [13]. A comparison of Figs. 6 and 5(b) shows that the X value at which the maximum temperature is attained is nearer to the axis origin for $l/2 = 10$ than for $l/2 = 1$. As far as the XZ planc is concerned, upstream temperature profiles at $l/2 = 10$ (Fig. 6) are very similar to those at $l/2 = 1$ [Fig. 5(b)], whereas downstream profiles are markedly different, since the wider the solid the less the effect of the adiabatic edge walls on the temperature gradient component along Y.

The axial coordinate at which the maximum midplane temperature is attained, $\bar{X}$, as a function of the depth, at different values of Peclet number and solid width, are presented for $H = 1$ and $H = 10$ in Figs. 7 and 8, respectively. Values were obtained by equating to zero the derivative of equation (18) and solving by means of the cut-and-try method. As far as the $H = 1$ case is concerned, one can see that the maximum temperature is attained asymptotically at $Z = 0.50$ for $l/2 = 0.1$ [Fig. 7(a)] and at $Z = 0.56$ for $l/2 = 1$ [Fig. 7(b)]. The $|\bar{X}|$ distributions in a thermally narrow solid [Fig. 7(a)] are very similar to those obtained in ref. [22] for a two-dimensional temperature distribution $T(X, Z)$ in an equally thick body. Figure 7(a) shows that at the upper surface the distance of the maximum from the origin decreases with increasing Peclet numbers. In the inside of the solid, near the upper surface, the higher the Peclet number the higher the variation of $|\bar{X}|$ with Z, since the higher the Peclet number the higher the ratio between the convective and the diffusive contributions to the heat removal. The Z asymptotic value at which the maximum midplane temperature is attained increases with increasing $l/2$, while temperature gradient components along Y determine a different effect at $Y = l/2$. In fact, when $l/2 = 0.1$ the asymptotic value is achieved at the same depth as at $Y = 0$, whereas it is attained at $Z = 0.44$ when $l/2 = 1$. Finally, Fig. 7(c) points out that, in a thermally wide body ($l/2 = 10$), maximum midplane temperatures are achieved also on the bottom surface ($Z = 1$), since temperatures in the midplane region are higher than those in the lateral zones, the thermal width of the solid being far higher than its thermal depth.

Figure 8 points out that, in a thermally thicker body ($H = 10$), the higher the Peclet number the greater the distance from the origin at which the maximum temperature is attained at any depth. A comparison of Figs. 7 and 8 shows for all width values that, when the diffusive contribution to the heat removal is greater than the convective one ($Pe = 0.1$), a higher thickness of the solid ($H = 10$ vs $H = 1$) enhances the diffusion of the heat along the depth and the width, in addition to that diffused along X, both upstream and downstream. This determines the displacement toward the origin of the maximum temperature point at the upper surface. Instead, when the diffusive con-

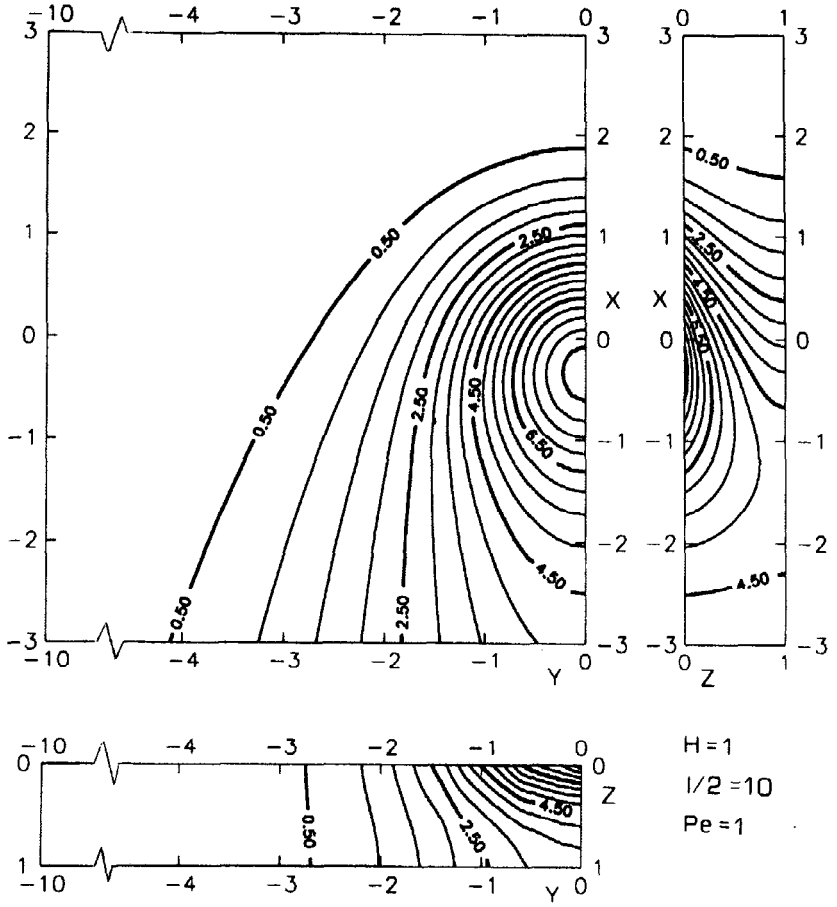

Fig. 6. Spatial distribution of the dimensionless temperature for $H = 1$, $l/2 = 10$ and $Pe = 1$.

tribution is negligible ($Pe = 10$), we can notice that the distance of the aforementioned point from the origin is nearly independent of the thickness of the solid. Figure 8 shows that, in a thermally thick body, the midplane maximum temperature is always achieved asymptotically. For $l/2 = 0.1$ and $l/2 = 1$ it is attained in the mid-depth plane ($Z = 5.0$), since in the former case the temperature distribution changes from a three-dimensional into a two-dimensional one within $Z < 1$, whilst in the latter one the thermal field is two-dimensional for any Z. In a thermally wider solid ($l/2 = 10$) asymptotic values of the temperature are achieved in the very deep part of the body.

Maximum midplane surface temperature axial coordinate as a function of Peclet number for $H = 1$, at different width values, has been plotted in Fig. 9. For $l/2 = 0.1$ and $l/2 = 1$, up to $Pe = 2$, the higher the Peclet number the nearer to the origin the $\bar{X}$ coordinate at which the maximum temperature is attained. For $l/2 = 0.1$ the higher the Peclet number the less $|\bar{X}|$, since increasing Peclet numbers determine a decrease of the temperature gradient component along X, whereas they practically do not affect the gradient component along Z. As a consequence, the maximum temperature point shifts toward the axis origin with increasing Pe. A similar behavior is shown for $l/2 = 1$, but in this case $|\bar{X}|$ values are less than the previous ones, since in the wider body there is a temperature gradient component along Y. Furthermore, we can notice that in the narrowest solid ($l/2 = 0.1$) at greater Pe values, after slightly increasing, $|\bar{X}|$ tends to a constant value. The effect of the temperature gradient component along Y turns out to be significant at the highest solid width ($l/2 = 10$) where $|\bar{X}|$ increases monotonically with increasing Peclet number, as expected in a thermally wide body.

The dimensionless midplane maximum temperature, T_{max}, as a function of the depth, at various Peclet numbers, for $H = 1$ and $l/2 = 1$, is reported in Fig. 10. Figure 10 points out that, the higher the Peclet number, the higher the dependence of maximum temperature on depth. Knowing the trend of the maximum temperature variation is very useful to those interested in heat treatments, such as hardening. As a matter of fact the figure shows that at $Pe = 1$ hardening depth is still highly dependent on deviations

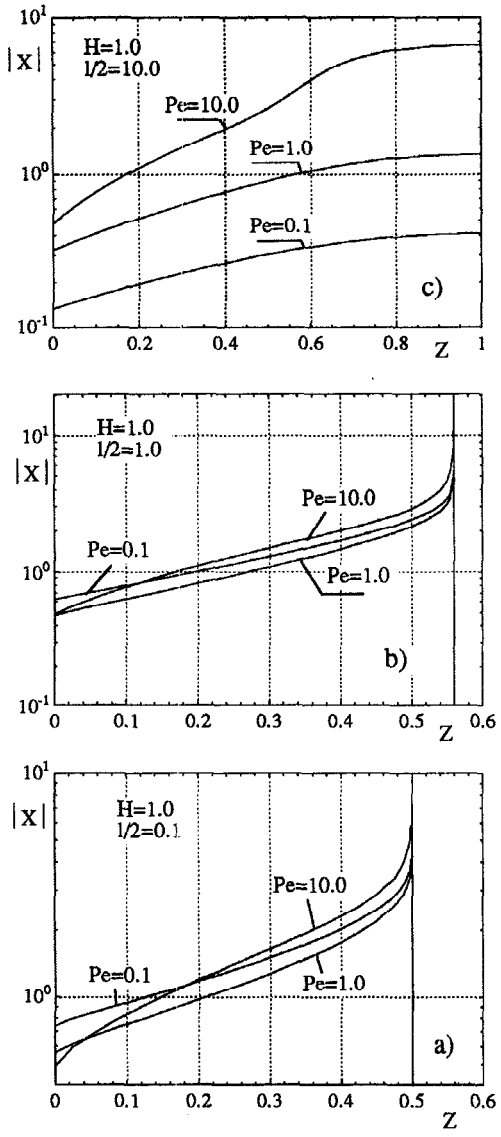

Fig. 7. Maximum midplane temperature axial coordinate ($Y = 0.0$) vs depth for $H = 1$, at different Peclet number values: (a) $l/2 = 0.1$; (b) $l/2 = 1$; (c) $l/2 = 10$.

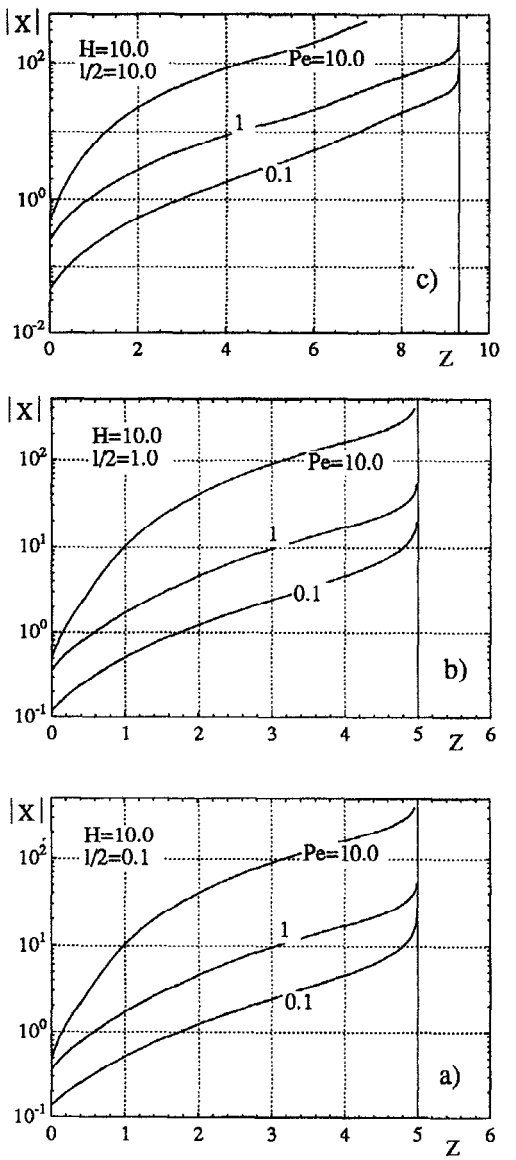

Fig. 8. Maximum midplane temperature axial coordinate ($Y = 0.0$) vs depth for $H = 10$, at different Peclet number values: (a) $l/2 = 0.1$; (b) $l/2 = 1$; (c) $l/2 = 10$.

of the maximum temperature from the hardening temperature. Helpful information about process parameters is also given by Fig. 11, where dimensionless midplane upper surface maximum temperature as a function of the Peclet number, for $H = 1$ and various width values, has been plotted. It is then easy to check whether or not melting temperature will be achieved on the top surface of the body during a heat treatment. The figure shows that up to about $Pe = 1$ the variation of T_{max} with Pe is lower in the thermally wider solid and that at high Peclet numbers the maximum temperature is nearly independent of them.

CONCLUSIONS

The temperature field in a solid whose width is far higher than the radius of Gaussian spot can be assumed to be two-dimensional at any thickness of the body. In fact, the temperature distribution for $l/2 = 0.1r$ is in good agreement with that derived in ref. [22]. Results showed that in a solid whose thickness is one tenth the radius of Gaussian spot, thermal gradients along the depth are negligible; in the worst case ($Pe = 10$ and $l/2 = 0.1r$) the midplane temperature on the bottom surface differs from that on the top surface by no more than 14%. Such a body can be considered thermally thin. The solution to the three-dimensional problem was in good agreement with that for an indefinite plate [13].

In a solid whose thickness and width are far lower than the radius of Gaussian spot the temperature distribution exhibits no maximum. Whatever the width,

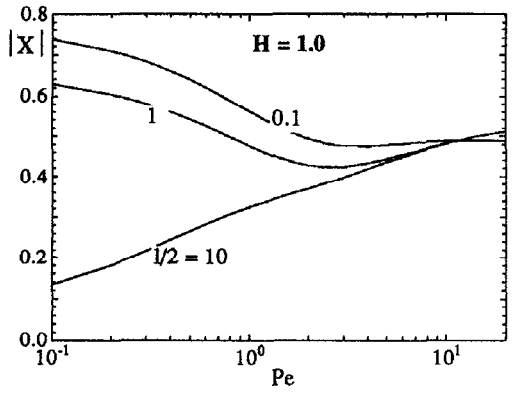

Fig. 9. Maximum midplane surface temperature axial coordinate ($Y = Z = 0.0$) vs Peclet number for $H = 1$, at different width values.

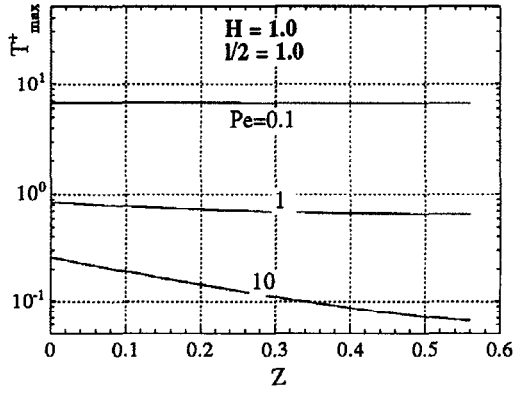

Fig. 10. Maximum midplane temperature ($Y = 0.0$) vs depth for $H = 1$ and $l/2 = 1$, at different Peclet numbers.

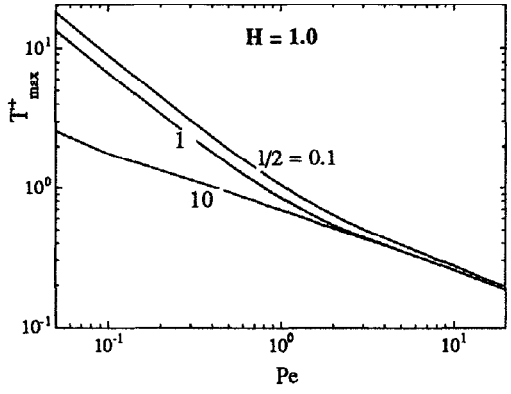

Fig. 11. Maximum midplane upper surface temperature ($Y = Z = 0.0$) vs Peclet number for $H = 1$, at different width values.

in a thermally thick body ($H = 0.1r$) the higher the Peclet number the greater the distance from the origin at which the asymptotic value of the upper surface temperature is attained, likewise in a semi-infinite solid. On the contrary, when $H = r$ and $l/2 = 0.1r$ as well as $l/2 = r$, maximum midplane surface temperature shifts toward the axis origin with increasing Peclet numbers up to about $Pe = 4$. Results also showed that, in a solid whose thickness and width are thermally finite ($H = l/2 = r$), the maximum midplane temperature is nearly independent of the depth when the diffusive contribution to the heat removal is far higher than the convective one ($Pe = 0.1$), whilst the maximum temperature on the top surface is much greater than that on the bottom surface when $Pe = 10$. One can therefore conclude that the lowest Peclet numbers are suitable for processes such as cutting and welding, whereas the highest Peclet numbers fit localized heat treatment such as hardening. Finally, it is worth noticing that, for $H = r$ and $Pe > 5$, the maximum midplane temperature on the top surface can be assumed to be independent of the width with an approximation not lower than 10%.

Acknowledgements—The Consiglio Nazionale delle Ricerche funded this work with grant no. 93.00640.

REFERENCES

1. R. K. Shah, H. Md. Roshan, V. M. K. Sastri and K. A. Padmanabhan (Eds), *Thermomechanical Aspect of Manufacturing and Materials Processing*. Hemisphere, Washington, DC (1992).
2. I. Tanasawa and N. Lior (Eds), *Heat and Mass Transfer in Materials Processing*, Hemisphere, Washington, DC (1992).
3. J. C. Jaeger, Moving sources of heat and temperature at sliding contacts, *Proceedings of the Royal Society of N.S.W.*, Vol. 76, pp. 203–224 (1942).
4. D. Rosenthal, The theory of moving sources of heat and its application to metal treatments, *Trans. ASME* **68**, 849–866 (1946).
5. H. S. Carslaw and J. C. Jaeger, *Conduction of Heat in Solids* (2nd Edn). Oxford University Press, Oxford (1959).
6. H. E. Cline and T. R. Anthony, Heat treating and melting material with a scanning laser or electron beam, *J. Appl. Phys.* **48**, 3895–3900 (1977).
7. I. Chen and S. Lee, Transient temperature profiles in solids heated with scanning laser, *J. Appl. Phys.* **54**, 1062–1066 (1983).
8. D. J. Sanders, Temperature distributions produced by scanning Gaussian laser beam, *Appl. Opt.* **23**, 30–35 (1984).
9. M. F. Modest and H. Abakians, Heat conduction in a moving semi-infinite solid subjected to pulsed laser irradiation, *J. Heat Transfer* **108**, 597–601 (1986).
10. Y. I. Nissim, A. Lietoila, R. B. Gold and J. F. Gibbons, Temperature distributions produced in semiconductors by a scanning elliptical or circular CW laser beam, *J. Appl. Phys.* **51**, 274–279 (1980).
11. J. E. Moody and R. H. Hendel, Temperature profiles induced by a scanning CW laser beam, *J. Appl. Phys.* **53**, 4364–4371 (1982).
12. L. G. Pittaway, The temperature distributions in thin foil and semi-infinite targets bombarded by an electron beam, *Br. J. Appl. Phys.* **15**, 967–982 (1964).
13. N. Lolov, Temperature field with distributed moving heat source, *International Institute of Welding*, Study Group 212, Doc. 212-682-87 (1987).
14. C. L. Tsai and C. A. Hou, Theoretical analysis of weld

pool behavior in the pulsed current GTAW process, *J. Heat Transfer* **110,** 160–165 (1988).
15. A. Kar and J. Mazumder, Three-dimensional transient thermal analysis for laser chemical vapor deposition on uniformly moving finite slabs, *J. Appl. Phys.* **65,** 2923–2933 (1989).
16. M. N. Ozisik, *Heat Conduction.* Wiley, New York (1980).
17. J. V. Beck, Green's function solution for transient heat conduction problems, *Int. J. Heat Mass Transfer* **27,** 1235–1244 (1984).
18. J. V. Beck, K. D. Cole, A. Haji-Sheikh and B. Litkouhi, *Heat Conduction Using Green's Functions.* Hemisphere, Washington, DC (1992).
19. M. Abramowitz and I. A. Stegun, *Handbook of Mathematical Functions with Formulas, Graphs and Mathematical Tables,* Applied Mathematics Series, Vol. 55. National Bureau of Standards, Washington, DC (1964).
20. R. Ghez, *A Primer of Diffusion Problem.* Wiley, New York (1988).
21. J. Spanier and K. B. Oldham, *An Atlas of Functions.* Hemisphere, New York (1987).
22. O. Manca, S. Nardini and V. Naso, Analytical solution to the temperature distribution in a finite depth solid with a moving heat source, *Proceedings of the 4th Brazilian Thermal Science Meeting,* pp. 287–291, Rio de Janeiro (1992).